Analyst

Accepted Manuscript

This is an *Accepted Manuscript*, which has been through the RSC Publishing peer review process and has been accepted for publication.

Accepted Manuscripts are published online shortly after acceptance, which is prior to technical editing, formatting and proof reading. This free service from RSC Publishing allows authors to make their results available to the community, in citable form, before publication of the edited article. This *Accepted Manuscript* will be replaced by the edited and formatted *Advance Article* as soon as this is available.

To cite this manuscript please use its permanent Digital Object Identifier (DOI®), which is identical for all formats of publication.

More information about *Accepted Manuscripts* can be found in the **Information for Authors**.

Please note that technical editing may introduce minor changes to the text and/or graphics contained in the manuscript submitted by the author(s) which may alter content, and that the standard **Terms & Conditions** and the **ethical guidelines** that apply to the journal are still applicable. In no event shall the RSC be held responsible for any errors or omissions in these *Accepted Manuscript* manuscripts or any consequences arising from the use of any information contained in them.

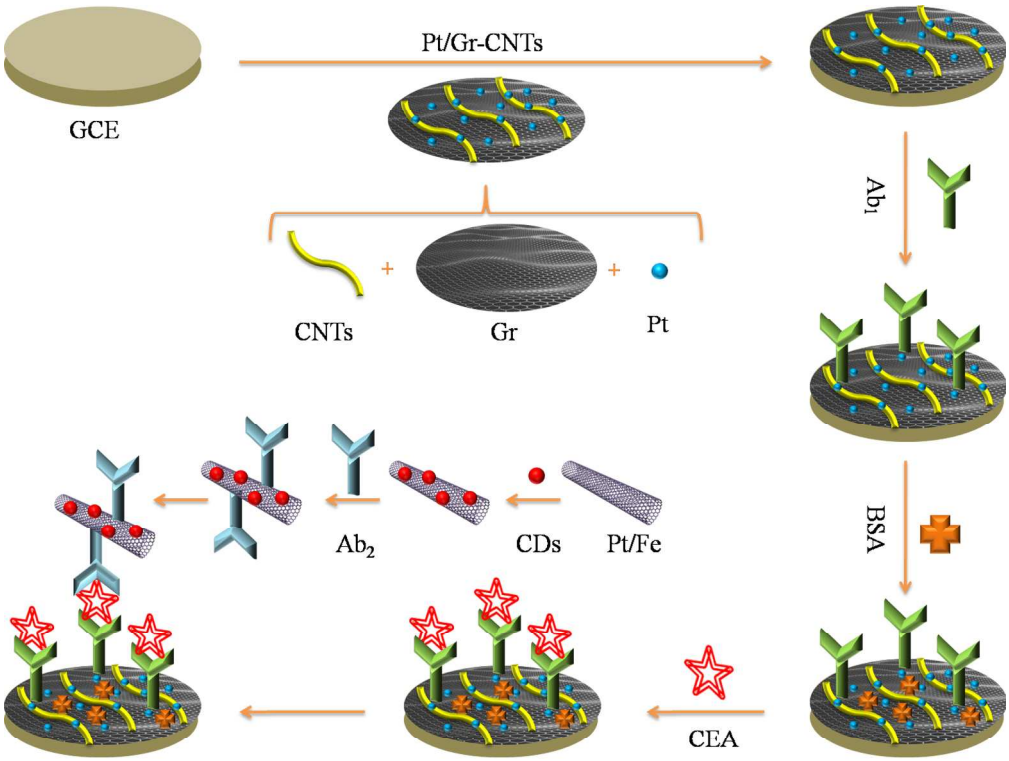

The immunosensor used Pt nanoparticles dotted graphene-carbon nanotubes composites (Pt/Gr-CNTs) as platform and carbon dots functionalized Pt/Fe nanoparticles (Pt/Fe@CDs) as bionanolabels

Graphical Abstract
254x238mm (300 x 300 DPI)

Dual amplification strategy for ultrasensitive electrochemiluminecence immunoassay based on Pt nanoparticles dotted graphene-carbon nanotubes composite and carbon dots functionalized mesoporous Pt/Fe

Wenping Deng,[a] Fang Liu,[a] Shenguang Ge,[b] Jinghua Yu,[a] Mei Yan,[a]* Xianrang Song[c]

[a]*Key Laboratory of Chemical Sensing & Analysis in Universities of Shandong, School of Chemistry and Chemical Engineering, University of Jinan, Jinan 250022, P.R. China*

[b]*Shandong Provincial Key Laboratory of Preparation and Measurement of Building Materials, University of Jinan, Jinan 250022, PR China*

[c]*Cancer Research Center, Shandong Tumor Hospital, Jinan 250012, P.R. China*

*Corresponding authors: Mei Yan

E-mail: chm_yanm@ujn.edu.cn (M. Yan)

Telephone: +86-531-82767161

ABSTRACT

A facile and sensitive electrochemiluminescence (ECL) immunosensor for detection of human carcinoembryonic antigen (CEA) was designed. The immunosensor used Pt nanoparticles dotted graphene-carbon nanotubes composites (Pt/Gr-CNTs) as platform and carbon dots functionalized Pt/Fe nanoparticles (Pt/Fe@CDs) as bionanolabels. Pt/Gr-CNTs was first synthesized using a facile ultrasonic method to modify working electrode, which can increase the surface area to capture a large amount of primary anti-CEA antibodies as well as improve the electronic transmission rate. The bionanolabels Pt/Fe@CDs prepared through ethanediamine linking, showed good ECL signal amplification performance. The reason was that Pt/Fe@CDs nanocomposites as signal tags could increase CDs loading per immunoreaction in comparation with single CDs. The approach provided a good linear response range from 0.003 to 600 $ng \cdot mL^{-1}$ with a low detection limit of 0.8 $pg \cdot mL^{-1}$. The immunosensor showed good specificity, acceptable stability and reproducibility. Satisfactory results were obtained for determination of CEA in human serum albumin samples. Hence, the proposed ECL immunosensor could become a promising method for tumor marker detection.

Keywords: Electrochemiluminescence; Pt nanoparticles dotted graphene-carbon nanotubes composite; Carbon dots functionalized Pt/Fe nanoparticles; Sandwich-type immunosensor

1. Introduction

The levels of tumor markers in blood or tissue provide essential information for clinical cancer screening and disease diagnosis.[1, 2] Electrochemiluminescence (ECL) immunoassay has shown promise in fast, selective, and sensitive detection of tumor markers with simple instrumentation in recent years.[3–6] Recently great efforts have been made to develop ultrasensitive immunosensors. Signal amplification is the most popular strategy that has been employed for the development of ultrasensitive immunoassay methods. Successful signal amplification strategies include applying new redox-active probes, coupling amplification-by-polymerization concepts with ECL detection, integrating enzyme-assisted signal amplification processes, and incorporating nanomaterials to increase loading of tags, etc.[7-13] Bionanocomposites with a high content of detection tags for signal tracing[14–19] have attracted special interests due to the outstanding optical, electronic, and biocompatible performance of nanoparticles.

At first, the nanotechnology revolution has been making a ground-breaking impact on diverse science, engineering, and commercial sectors, including the construction industry. The nanomaterials with unique physical and chemical properties, such as quantum dots[20, 21] and metal nanoparticles,[22–24] have been widely used. For example, Pt nanoparticles (Pt NPs) are the popular and effective conductive materials. To further enhance the conductivity of Pt NPs and lower the use of Pt NPs, it is highly desirable to load Pt NPs on the surface of suitable supporting materials. Many articles have referred to synthesis of carbon nanotubes as supports. In this paper,

to further improve the conductivity and increasing surface-to-volume ratio, we proposed a new and simple method to make Pt NPs assemble onto the graphene-carbon nanotubes composite (Pt/Gr-CNTs). Great improvements have been made in these materials due to their unusual intercalation property, excellent electrical conductivity and high surface-to-volume ratio. In addition, a simple ultrasonic method was first reported to synthesize Pt/Gr-CNTs in our work. In short, this hybrid nanomaterial possesses so many advantages, such as easy preparation, excellent separation function, high electrical conductivity, high surface-to-volume ratio, and good biocompatibility, so it was selected as sensing platform to immobilize primary anti-CEA antibodies (Ab_1).

What's more, to further improve the ECL performance and achieve much higher sensitivity, we employed mesoporous Pt/Fe nanoparticles coated with carbon dots (Pt/Fe@CDs) as signal tags. The nanocomposite could increase carbon dots (CDs) loading per immunoreaction in comparison with single CDs. Mesoporous nanoparticles Pt/Fe have many unique structural features compared with other solid nanoparticles, including large surface area and high pore volume, ordered porous channels, uniform and tunable pore structure. These characteristics have the virtue of conjugating more biomolecules, and improving the sensitivity of bioanalysis. At the same time, the hierarchical nanoporous Pt/Fe alloy has superior structure stability compared to Pt NPs, holding promising application potential. The conductivity of porous nanomaterials can be well applied by doping electroluminescent substance into the pores with an in situ synthesized method. In addition, CDs are low cytotoxicity,

excellent water-solubility, and easy surface modification. The unique properties of Pt/Fe@CDs provide a promising platform for the development of high-performance ECL immunosensors.

Herein, we designed a sensitive ECL immunosensor for carcinoembryonic antigen (CEA) detection via self-assembly based on Pt/Gr-CNTs modified glassy carbon electrode (GCE). It constructed an effective antibody immobilization matrix and made the immobilized immunocomponents possess high stability and bioactivity. In addition, the sensitivity was enhanced by using Pt/Fe@CDs as signal labels. Ab_1 and the secondary anti-CEA antibodies (Ab_2) were covalently bonded to Pt/Gr-CNTs and Pt/Fe@CDs nanocomposite, respectively, to fabricate a sandwich-type immunosensor, as shown in Scheme 1. The experimental results indicated that the prepared immunosensor exhibited simple instrumentation, high sensitivity, wide linear range and excellent analytical performance.

2. Experimental section

2.1. Reagents

Multiwalled carbon nanotubes (CNTs, CVD method, purity ≥98 %, diameter 60–100 nm, and length 1–2 μm) were purchased from Nanoport Co. Ltd. (Shenzhen, China). The natural graphite powder was obtained from J&K Scientific Ltd. Ethylene glycol (EG) was obtained from Tianjin Guangcheng chemical reagent Co. Ltd. (Tianjin, China). Chloroplatinic acid (H_2PtCl_6) was bought from Shanghai Chemical Reagent Company (Shanghai, China). Ethanediamine, graphite flake, the commercial Johnson Matthey Pt/C catalyst (20 wt. %),

N-(3-dimethylaminopropyl)-N'-ethylcarbodiimi- dehydro-chloride (EDC) and N-hydro-xysuccinimide (NHS) were purchased from Alfa Aesar. Carcinoembryonic antigen standard solutions, the primary anti-CEA and the secondary anti-CEA were bought from Shanghai Linc-Bio Science Co. LTD (Shanghai, China). Bovine serum albumin (BSA, 96–99 %) was obtained from Sigma (St. Louis, MO, USA). Phosphate buffered solutions (PBS, 0.01 mol·L^{-1}, pH 7.4) containing 0.1 mol·L^{-1} $K_2S_2O_8$ and 0.1 mol·L^{-1} KCl was used as the electrolyte. The clinical serum samples were from Jiangsu Institution of Cancer Research. Ultrapure water obtained from a Millipore water purification system (≥18 MΩ cm, Milli-Q, Millipore) was used in all assays. All other reagents were of analytical grade and used as received.

2.2. Apparatus

The ECL measurements were carried out on a MPI-E multifunctional electrochemical and chemiluminescence analytical system (Xi'an Remex Analytical Instrument Ltd. Co.) biased at 800 V. UV-vis absorption spectra were recorded on a UV-2550 spectrophotometer (Shimadzu, Japan). The fluorescent properties were tested on a RF-5301pc spectrofluorophotometer (Shimadzu, Japan). Cyclic voltam-metric measurements (CVs) were performed with a CHI 760D electrochemical workstation (Shanghai CH Instruments, China). Scanning electron microscopy (SEM) images were obtained from QUANTA FEG 250 thermal field emission scanning electron microscopy (FEI Co., USA) and energy dispersive spectrometer (EDS) was obtained using a Oxford X-MAX50EDS (Oxford, Britain). Electrochemical impedance spectroscopy (EIS) was carried out on an IM6X

electrochemical station (Zahner, Germany). All experiments were carried out with a conventional three-electrode system with the modified glassy carbon electrode (GCE, 3 mm in diameter) as the working electrode (WE), a platinum counter electrode (CE) and an Ag/AgCl (sat. KCl) reference electrode (RE).

2.3. Preparation of the Ab_2-Pt/Fe@CDs labels

Nanoporous Pt/Fe Alloy, used as carriers for CDs immobilization, was synthesized with previously reported seed-growth method.[25, 26] $Pt_{11}Fe_9Al_{80}$ (atomic %) ternary alloy foils were prepared by refining pure (>99.9 %) Pt, Fe, and Al in an arc furnace, followed by melt-spinning under an argon-protected atmosphere. NP-$Pt_{55}Fe_{45}$ alloy and Pt NPs were prepared by selectively etching the $Pt_{11}Fe_9Al_{80}$ and $Pt_{20}Al_{80}$ alloys in 2.0 M NaOH solution for 48 h at room temperature, respectively. During the preparation of carbon-supported PtFe/C nanoparticles, Vulcan XC-72 carbon black was pretreated in 6 M HNO_3 solution at 100 °C for 4 h[27] and a feeding mole ratio between platinum and iron is controlled at 55:45. The procedure was operated completely according to the work by Xu et al.[28]

Preparation of carbon dots (CDs). CDs were prepared in an ECL cell in pH 7.0 PBS consisting of a graphite rod WE, a Pt mesh CE, an Ag/AgCl RE. The applied potential at the graphite rod electrode was cycled between -3.0 V and 3.0 V at 0.1 $V \cdot s^{-1}$. Carbon structure of the CDs ensures it to be an ideal candidate as nanosupports for biomolecules immobilization and biosensor fabrication.

Fabrication of CDs coated nanoporous Pt/Fe Alloy (Pt/Fe@CDs). 200μL of freshly prepared EDC (10 $mg \cdot mL^{-1}$, in 0.1 M pH 7.4 PBS) and 100 μL of NHS (10

mg·mL^{-1}, in 0.1 M pH 7.4 PBS) were added to 500 μL of CDs, After sonicating for 2 h, the suspension was centrifuged and washed with ethanol repeatedly for two times, and the carboxyl-activitied nanoparticles were obtained. Simultaneously, 100μL of Pt/Fe was first dispersed in 0.5 mL of ethanediamine and sonicated 1 hour to obtain a homogeneous dispersion. The suspension was centrifuged and washed with ethanol repeatedly for two times. Then, the carboxyl-functionalized nanoparticles were dispersed in it. After stirring for 30 min, unbound CDs were removed by successive centrifugation and washed with ethanol several times.

Constitution of Pt/Fe@CDs composites labeled Ab_2. Ab_2 with $–NH_2$ can directly conjugate with carboxyl-activitied CDs. Briefly, 1 mL of the above Pt/Fe@CDs suspension was mixed with 1 mL of Ab_2 solution (anti-CEA, 20 μg·mL^{-1}, in 0.01 M pH 7.4 PBS). After stirring for 30 minutes, free antibody was removed by centrifugation and washed with 0.01 M PBS for several times to obtain the Pt/Fe@CDs nanoparticles labeled Ab_2 (Ab_2-Pt/Fe@CDs). Then was incubated in 1 wt % BSA for 40 minutes to block non-specific binding sites.

2.4. Preparation of Pt/Gr-CNTs composites

Preparation of graphene oxide (GO). GO was prepared from natural graphite by a modified Hummers method.[29, 30]

Constitution of acid-treated carbon nanotubes (CNTs). The CNTs was purified by refluxing CNTs in 60 % HNO_3 at 60 °C for 6 h to remove the metal particles and other impurities. After the purification process, the surface oxidation of the CNTs was carried out by refluxing CNTs in 1:1 conc. H_2SO_4 and conc. HNO_3 at 60 °C for 24 h.

Fabrication of Pt/Gr-CNTs composites. The aqueous colloidal suspensions of GO nanosheets were then poured into the CNTs conglomerations, and the mixture was then sonicated for 2 h. This suspension was centrifuged for 15 minutes at 3000 rpm to remove the unstabilized CNTs, giving a suspension of the GO-CNTs nanocomposites and the excess GO remained in the supernatant. Next, the GO-CNTs nanocomposites were separated from the excess GO sheets by repeating centrifugation (10,000 rpm, 20 minutes) and water washing steps. After that, 10 mg GO-CNTs was added into 0.25 mL aqueous solution containing 38.6 mM H_2PtCl_6, and then the mixture was ultrasonically treated for 1 h to form a stable colloid. Sequentially, 2 mL of EG was injected into the mixture with magnetic stirring for 1 h and then ultrasonicing 1.5 h. The final Pt/Gr-CNTs composites were collected by filtration, and washed with deionized water.

2.5. Fabrication of the ECL immunosensor via sandwich mode

The whole process for construction of the modified electrode was shown schematically in Scheme 1. Firstly, 5 μL of Pt/Gr-CNTs composite solution was dropped on the GCE and dried at room temperature. After washing with pH 7.4 PBS, 5 μL of 20 $\mu g \cdot mL^{-1}$ Ab_1 (0.01 $mol \cdot L^{-1}$ PBS, pH 7.4) was applied to the corresponding WE and reacted at room temperature for 30 minutes. Pt connected with $-NH_2$ of Ab_1.[31] After that, excess antibodies were washed with pH 7.4 PBS and incubated in 1 wt % BSA for 40 minutes to block non-specific binding sites. Subsequently, the electrode was incubated with various concentrations of CEA solution. Finally, the

as-prepared Ab_2-Pt/Fe@CDs composites were dropped on to the modified electrode surface, followed by washing, and used for the CEA detection.

2.6. ECL detection of CEA with the immunosensor

ECL measurements were done at room temperature and the potential swept from -0.5 V to -1.5 V with a scan rate of 100 $mV \cdot s^{-1}$. The ECL measurements were performed in a solution of 0.01 $mol \cdot L^{-1}$ PBS containing 0.1 $mol \cdot L^{-1}$ $K_2S_2O_8$ and 0.1 $mol \cdot L^{-1}$ KCl with a photomultiplier tube voltage of 800 V. The ECL signals related to the CEA concentrations could be measured.

3. Results and discussion

3.1. SEM and TEM characterization of Gr-CNTs, Pt/CNTs and Pt/Gr-CNTs

Detailed verification of the Gr-CNTs, Pt/CNTs, Pt/Gr-CNTs morphology is performed by SEM and EDS analysis in Fig. 1. It is shown that the individual CNTs are uniformly attached to the Gr without agglomeration (Fig. 1A). The morphology of the as-prepared Gr shows a thin sheet shape. It is also confirmed that the CNTs are well dispersed onto Gr without any appreciable aggregations in each Gr-CNTs composite. Fig. 1B and Fig. 1C show the SEM images and EDS of Pt/CNTs, respectively. It is interesting to see that the Pt NPs preferentially adhere to the surfaces of CNTs rather than to other regions without CNTs. And it shows the diameter of the CNTs was about 35–45 nm. The SEM image of Pt/Gr-CNTs (Fig. 1D) show that highly dispersed Pt NPs are uniformly distributed on Gr-CNTs. EDS pattern of Pt/Gr-CNTs is shown in Fig. 1E and Fig. 1F. According to the results

obtain from SEM and EDS, it can be concluded that Pt NPs are successfully deposited on the surface of the Gr-CNTs composite.

3.2. Characterization of Pt/Fe@CDs

As shown in Fig. 2A, the resulted structure is composed of many interconnected larger ligaments, with the diameter in the range of 100−150 nm, within which a number of irregular pores formed. And from the SEM image, it is interesting to find that these large ligaments themselves have 3D bicontinuous spongy morphology with a narrow ligament size at 3 nm. To better understand the influence of CDs, we performed the fluorescence characterization. And in the fluorescent spectra, respectively, Pt/Fe@CDs and CDs of maximal emission wavelengths are 414 nm and 469 nm. As shown in Fig. 2B, a small blue shift of Pt/Fe@CDs (curve b) is observed in contrast with that of the individual CDs (curve a). This suggested that CDs and Pt/Fe alloy are combined with strong chemical bonds force[32, 33], confirming the successful preparation for the composite of Pt/Fe@CDs.

3.3. EIS characterization of the CEA sensor

EIS is an effective method for probing the features of surface-modified electrodes. The impedance spectra include a semicircle portion and a linear portion. The semicircle diameter at higher frequencies corresponds to the electron-transfer resistance (R_{et}), and the linear part at lower frequencies corresponds to the diffusion process. Fig. 3 shows the EIS of the GCE at different modification stages. It is observed that the EIS of the bare electrode displayed an almost straight line (curve a), which is characteristic of a mass diffusion limiting process. After the GCE were

coated by the Pt/Gr-CNTs composite, the impedance decreased, thus showing a smaller R_{et} (curve b). Similarly, Ab_1, BSA, CEA and Pt/Fe@CDs-Ab_2 could all resist the electron-transfer kinetics of the redox probe at the electrode interface, resulting in the increased impedance of the electrode (curves c-f), which verifies the immobilization of these substances. However, the impedance of the Pt/Fe@CDs-Ab_2 increases slightly, because of the Pt/Fe possesses good electron transfer efficiency. Hence the tendency of increase with the impedance is retarded.

3.4. ECL behaviors of our immunoassay

The GCE were scanned from -0.5 V to -1.5 V with scan rate of 100 $mV \cdot s^{-1}$. To investigate the amplification technique of the Pt/Gr-CNTs and Pt/Fe@CDs composites for ECL analysis, we designed two experiments. One experiment was designed without the involvement of the Gr for the sensing platform, the other without the Pt/Fe alloy for the signal label. We compared the ECL intensity of only Pt/CNTs composites modified GCE and Pt/Gr-CNTs composites modified GCE (Fig. 4A). The quantity of the Pt/CNTs and Pt/Gr-CNTs composites is equal in both tags. Similarly, in the Fig. 4B, we compared the ECL intensity of pure CDs labeled Ab_2 and Pt/Fe@CDs composites labeled Ab_2. The quantity of labels is also equal. As can be seen in Fig. 4, the Pt/Gr-CNTs composites modified GCE reveals excellent ECL performance compared with only Pt/CNTs composites. The Gr-CNTs could display a higher surface-to-volume ratio than pure CNTs, which could enhance the immobilized amount of Pt NPs. The same is to Pt/Fe@CDs that the mesoporous Pt/Fe

nanoparticles could also increase the surface area, which could benefit for the immobilization of more CDs.

Adopting CDs as luminescent material, the ECL mechanism involves the formation of excited-state CDs (CDs^*) via electron-transfer annihilation of negatively charged ($CDs^{\bullet-}$) and positively charged CDs ($CDs^{\bullet+}$). The intensity of cathodic ECL was larger than that of anodic ECL, indicating that $CDs^{\bullet+}$ is more stable than $CDs^{\bullet-}$. Additionally, ECL obtained by using $S_2O_8^{2-}$ as a coreactant, suggesting attractive applications of CDs in ECL sensing. The ECL emission mechanism of CDs was similar to other ECL systems using peroxydisulfate as oxidative coreactant. The possible ECL mechanisms are as follows:[34]

$$CDs + e^- \rightarrow CDs^{\bullet-} \quad (1)$$

$$S_2O_8^{2-} + e^- \rightarrow SO_4^{2-} + SO_4^{\bullet-} \quad (2)$$

$$CDs^{\bullet-} + SO_4^{\bullet-} \rightarrow CDs^* + SO_4^{2-} \quad (3)$$

$$CDs^* \rightarrow CDs + h\nu \quad (4)$$

So we can see that the Pt/Gr-CNTs and the Pt/Fe@CDs composites can be used as excellent ECL.

3.5. Optimization of immunoreaction conditions

The ECL intensity of the immunosensor depends on some external conditions to some extends, such as applied potential, pH value and incubation time, so these conditions were selected as follows.

The potential affects the analytical performence in a way, hence different potentials were investigated in our work, and the ECL curves were obtained as the Fig. 5A. It can be observed that the optimal scanning potential is from -0.5 V to -1.5 V.

To the best of our knowledge, the chemical properties changes with the pH value, and the ECL intensity of the immunosensor in different acidity, was shown in Fig. 5B. Obviously, we select pH 7.4 as the optimal acidity when the pH value varied from 6.5 to 8.6.

Another influencing condition, which cannot be neglected, is the incubation time of Ab_1 and CEA. As shown in Fig. 5C, the ECL intensity increases with the increasing of the incubation time (T_1), and inclines to a constant value after 40 minutes, ascribing to the saturated binding between the analyte and the capture antibody.

Furthermore, the effect of the incubation time of CEA with Pt/Fe@CDs labeled Ab_2 (Fig. 5D) on the ECL intensity of the immunosensor is investigated, from which it can be seen that the optimal incubation time (T_2) is 40 minutes. The ECL intensity increases with the increasing of the incubation time, and inclines to a constant value after 40 minutes, ascribing to the saturated binding between the analyte and the capture antibody.

3.6. Analytical performance

Under the optimal conditions, a series of immunosensors were prepared for the detection of different concentrations of CEA. The ECL intensity response increases with the increasing of CEA concentration in the range of 0.003–600 $ng \cdot mL^{-1}$, the

equation of the calibration curve (Fig. 6) is $\Delta ECL = 5389.49 + 2235.2 \lg c_{CEA}$ (c_{CEA}/ng·mL^{-1}), with a correlation coefficient of 0.9989. The limit of detection (LOD) at a signal-to-noise of 3 is 0.8 pg·mL^{-1}. The results demonstrate that the proposed method could be used for the determination of CEA. Moreover, Table 1 shows the comparation of linear range and detection limit for immunosensors in previous reports and our proposed work.[35] The limit of detection for our immunosensor is much lower than those of 0.03–2.7 ng·mL^{-1} for the reported competitive immunosensors (Table 1). The low LOD and large line range may be attributed to two factors: 1) the intrinsic property of high surface-to-volume ratio of Gr-CNTs, which could greatly increase the loading of Pt NPs and Ab_1 due to its high surface area, as well as enhance the conductivity; 2) Nanoporous Pt/Fe alloy with a three-dimensional interconnected network structure in the nanoscale and the hollow channels embedded in the solid nanoarchitectures can immobilize more CDs to amplify signals; Besides, Pt/Fe alloy could appropriate decrease resistivity of Pt/Fe@CDs.

3.7. Specificity, stability and reproducibility of the immunosensor

To further characterize the specificity of the immunosensor, 1 ng·mL^{-1} CEA containing 20 ng·mL^{-1} human serum albumin (HSA), and 20 ng·mL^{-1} prostate protein antigen (PSA) was measured by the immunosensor. Compared with the ECL response of the immunosensor in 1 ng·mL^{-1} pure CEA, no significant difference is observed (Fig. 7A), indicating that the immunosensor displays good specificity for the determination of CEA.

The stability of the proposed ECL immunosensor was also examined by checking periodically their ECL intensity responses. After running for 10 cycles (Fig. 7B), only a 2.7 % decline of the original ECL was observed for the fabricated immunosensor, which demonstrated that the sensing layer of the immunosensor owned excellent stability. When the immunosensor was not in use, it was stored in refrigerator at 4 ℃. After half month, the ECL intensity of the immunosensor decreases to about 94 % of its initial value (Fig. 7C). The slow decrease in the ECL intensity demonstrates that the immunosensor had good stability.

The reproducibility of the immunosensor for CEA was estimated with intra- and inter-assay precision. The intra-assay precision was evaluated by assaying one CEA level for four replicate measurements. The inter-assay precision was estimated by determining one CEA level with four GCE immunosensors made at the same electrode. The intra- and inter-assay variation coefficients (VCs) obtained from 1 ng $\cdot mL^{-1}$ CEA are 6.2 % and 6.9 %, respectively. Obviously, the inter-assay VC shows a good electrode-to-electrode reproducibility of the fabrication protocol, while the low value of intra-assay VC indicates that the immunosensor could be regenerated and used repeatedly.

3.8. Application of the immunosensor in human serum

The feasibility of the immunoassay system for clinical applications was investigated by analyzing several real samples. In comparison with the enzyme-linked immunosorbent assay (ELISA) analysis, these serum samples were diluted to different concentrations with PBS of pH 7.4.

Table 2 describes the correlation between the results obtained by the proposed ECL immunosensor and the ELISA method. The recoveries from these two methods ranged from 97.7 to 103.6 % and 98.8 to 104.4 %, respectively. The relative deviation was lower than 3.0 %, indicating that there is no significant difference between the results and ELISA method. Thus, the developed immunosensor could be satisfactorily applied to the clinical determination of CEA levels in human serum.

4. Conclusion

An ultrasensitive ECL immunosensor for the detection of CEA was first developed using Pt/Fe@CDs as excellent ECL labels. The sandwich-type immunoreaction allows us to determine CEA down to 3 $pg \cdot mL^{-1}$ with high sensitivity and selectivity etc. The main advantages of the present immunosensor can be attributed to two aspects. First, the Pt/Gr-CNTs composite modified GCE could attach more antibodies and promote the electric transmission than pure CNTs or Gr, offering it to be an excellent sensing platform. Second, a novel ECL label of Pt/Fe@CDs composites was achieved with excellent ECL activity. It is evidenced that the trimodal hollow bimetallic structure in the nanotubular mesoporous Pt/Fe biometallic alloy plays a crucial role for the loading of the more CDs. As a result, the as-proposed ECL immunosensor exhibits excellent performances, such as good stability, amplification effect, and satisfactory analytical performance, etc. The ECL immunosensor may also be extended for the detection of other relative biomarkers, which is of great application potential in point-of-care applications for accurate clinical disease diagnostics.

Acknowledgements

This work was financially supported by National Natural Science Foundation of China (51003039, 51273084, 21277058) and Technology Development Plan of Shandong Province, China (Grant No. 2012GGB011813).

References

1 D. Sidransky, *Nat. Rev. Cancer*, 2002, **3**, 210.

2 J. D. Wulfkuhle, L. A. Liotta, E. F. Petricoin, *Nat. Rev. Cancer*, 2003, **3**, 267.

3 X. H. Li, L. Dai, Y. Liu, X. J. Chen, W. Yan, L. P. Jiang, J. J. Zhu, *Adv. Funct. Mater*., 2009, **19**, 3120.

4 J. A. Ho, Y. C. Lin, L. S. Wang, K. C. Hwang, P. T. Chou, *Anal. Chem.,* 2009, **4**, 1340.

5 H. G. Nie, S. J. Liu, R. Q. Yu, J. H. Jiang, *Angew. Chem. Int. Ed*., 2009, **48**, 9862.

6 R. Malhotra, V. Patel, J. P. Vaqué, J. S. Gutkind, J. F. Rusling, *Anal. Chem*., 2010, **82**, 3118.

7 Z. P. Chen, Z. F. Peng, Y. Luo, B. Qu, J. H. Jiang, X. B. Zhang, G. L. Shen, R. Q. Yu, *Biosen. Bioelectron.,* 2007, **23**, 485.

8 D. P. Tang, J. J. Ren, *Anal. Chem*., 2008, **80**, 8064.

9 J. Wang, W. Y. Meng, X. F. Zheng, S. L. Liu, G. X. Li, *Biosen. Bioelectron*., 2009, **24**, 1598.

10 S. S. Zhang, H. Zhong, C. F. Ding, *Anal. Chem*., 2008, **80**, 7206.

11 W. C. Mak, K. Y. Cheung, D. Trau, A. Warsinke, F. Scheller, R. Renneberg, *Anal. Chem*., 2005, **77**, 2835.

12 W. -C. Liao, J. A. Ho, *Anal. Chem*., 2009, **81**, 2470.

13 J. Wang, J. H. Li, A. J. Baca, J. B. Hu, F. M. Zhou, W. Yan, D. W. Pang, *Anal. Chem*., 2003, **75**, 3941.

14 J. Wang, G. Liu, M. R. Jan, *J. Am. Chem. Soc*., 2004, **126**, 3010.

15 X. Yu, B. Munge, V. Patel, G. Jensen, A. Bhirde, J. D. Gong, S. N. Kim, J. Gillespie, J. S. Gutkind, F. Papadimitrakopoulos, J. F. Rusling, *J. Am. Chem. Soc.,* 2006, **128**, 11199.

16 R. J. Cui, C. Liu, J. N. Shen, D. Gao, J. J. Zhu, H. Y. Chen, *Adv. Funct. Mater*., 2008, **18**, 2197.

17 L. Y. Chen, C. L. Chen, R. N. Li, Y. Li, S. Q. Liu, *Chem. Commun*., 2009, **19**, 2670.

18 V. Mani, B. V. Chikkaveeraiah, V. Patel, J. S. Gutkind, J. F. Rusling, *ACS Nano*., 2009, **3**, 585.

19 D. Du, Z. X. Zou, Y. Shin, J. Wang, H. Wu, M. H. Engelhard, J. Liu, I. A. Aksay, Y. Lin, *Anal. Chem*., 2010, **82**, 2989.

20 G. D. Liu, J. Wang, J. Kim, M. R. Jan, *Anal. Chem*., 2004, **76**, 7126.

21 J. Wang, G. D. Liu, H. Wu, Y. H. Lin, *Small,* 2008, **4**, 82.

22 J. A. Ho, H. C. Chang, N. Y. Shih, L. C. Wu, Y. F. Chang, C. C. Chen, C. Chou, *Anal. Chem*., 2010, **82**, 5944.

23 B. P. Ting, J. Zhang, M. Khan, Y. Y. Yang, J. Y. Ying, *Chem. Commun*., 2009, **41**, 6231.

24 G. S. Lai, J. Wu, H. X. Ju, F. Yan, *Adv. Funct. Mater*., 2011, **21**, 2938.

25 Y. F. Wu, C. L. Chen, S. Q. Liu, *Anal. Chem.,* 2009, **81**, 1600.

26 Caixia Xu, Qian Li, Yunqing Liu, Jinping Wang and Haoran Geng, *Langmuir,* 2011, **28**, 1886.

27 H. Zhao, L. Li, J. Yang, Y. Zhang, H. Li, *Electrochem. Commun*., 2008, **10**, 876.

28 J. Xu, K. Hua, G. Sun, C. Wang, X. Lv, Y. Wan, *Electrochem. Commun*., 2006, **8**, 982.

29 S. Stankovich, D. A. Dikin, G. H. B. Dommett, K. M. Kohlhass, Z. J. Zimney, E. A. Stach, R. D. Piner, S. T Nguyen and R. S. Ouff, *Nature,* 2006, **442**, 282.

30 K. S. Novoselov, Z. Jiang, Y. Zhang, S. V. Morozov, H. L. Stormer, U. Zeitler, J. C. Maan, G. S. Boebinger, P. Kim and A. K. Geim, *Science*, 2007, **315**, 1377.

31 S. Mandal, D. Roy, R. V. Chaudhari, M. Sastry, *Chem. Mater.* 2004, **16**, 3714.

32 R. Yuge, M. Zhang, M. Tomonari, T. Yoshitake, S. Lijima, M. Yudasaka, *ACS. Nano.,* 2008, **2**, 1865.

33 C. Q. Ding, A. W. Zhu, Y. Tian, *Acc. Chem. Res.,* 2013, DOI: 10.1021/ar400023s.

34 L. Zheng, Y. Chi, Y. Dong, J. Lin and B. Wang, *J. Am. Chem. Soc*., 2009, **131**, 4564.

35 J. Wu, Y. T. Yan, F. Yan and H. X. Ju, *Anal. Chem.,* 2008, **80**, 6072.

36 F. Tan, F. Yan, H. Ju, *Electrochem. Commun*., 2006, **8**, 1835.

37 J. Wu, J. Tang, Z. Dai, F. Yan, H. Ju, N. E. Murr, *Biosens. Bioelectron*., 2006, **22**, 102.

38 X. Li, R. Yuan, Y. Chai, L. Zhang, Y. Zhuo, Y. J. Zhang, *Biotechnol*., 2006, **123**, 356.

39 J. Pan, Q. Yang, *Anal. Bioanal. Chem*., 2007, **388**, 279.

40 D. Tang, R. Yuan, Y. J. Chai, *Phys. Chem. B*., 2006, **110**, 11640.

Figure Captions

Scheme 1. Schematic representation of the fabrication of the ECL immunosensor.

Fig. 1 Characterization of Gr-CNTs, Pt/CNTs and Pt/Gr-CNTs: Representative SEM images of Gr-CNTs (A), Pt/CNTs (B), and Pt/Gr-CNTs (D), EDS of Pt/CNTs (C), and Pt/Gr-CNTs (E and F).

Fig. 2 SEM of Pt/Fe alloy (high-magnification SEM image of Pt/Fe alloy in insert figure) (A), and PL spectra (B) of CDs (curve a) and Pt/Fe@CDs (curve b).

Fig. 3 EIS of bare GCE (a), GCE/Pt/Gr-CNTs (b), and GCE/Pt/Gr-CNTs-Ab_1 before (c) and after (d) blocking with BSA in 0.01 M PBS (2.5 mM $Fe(CN)_6^{4-/3-}$ + 0.1 M KCl, pH 7.4). (e) CEA/BSA/Ab_1-Pt/Gr-CNTs/GCE; (f) Pt/Fe@CDs-Ab_2/CEA/BSA/Ab_1-Pt/Gr-CNTs/GCE. The frequency range is between 0.01 Hz and 100000 Hz with signal amplitude of 5 mV.

Fig. 4 Comparison of different immunoassays with different immunocomplexes: Pt/Gr-CNTs-Ab_1-CEA-Ab_2-Pt/Fe@CDs (a, c), Pt-CNTs-Ab_1-CEA-Ab_2-Pt/Fe@CDs (b), Pt/Gr-CNTs-Ab_1-CEA-Ab_2-CDs (d).

Fig. 5 Effect of potential (A), pH (B), T_1 (C) and T_2 (D) on the ECL intensity.

Fig. 6 ECL profiles of the ECL immunosensor in the presence of different concentrations of CEA in PBS containing 0.1 M KCl and 0.1 M $K_2S_2O_8$. Inset:

456 calibration curve for CEA determination. CEA determination ($ng \cdot mL^{-1}$): 0 (a), 0.003

457 (b), 0.01 (c), 0.1 (d), 1.0 (e), 10.0 (f), 100.0 (g), 600.0 (h).

458 Fig. 7 Specificity (A) and stability (B and C) of the immunosensor.

459 **Table Captions**

460 Table 1. Analytical properties of different CEA electrochemical immunosensors.

461 Table 2. Comparison of CEA detection between the proposed immunosensor and

462 ELISA methods in CEA-spiked human serum samples.

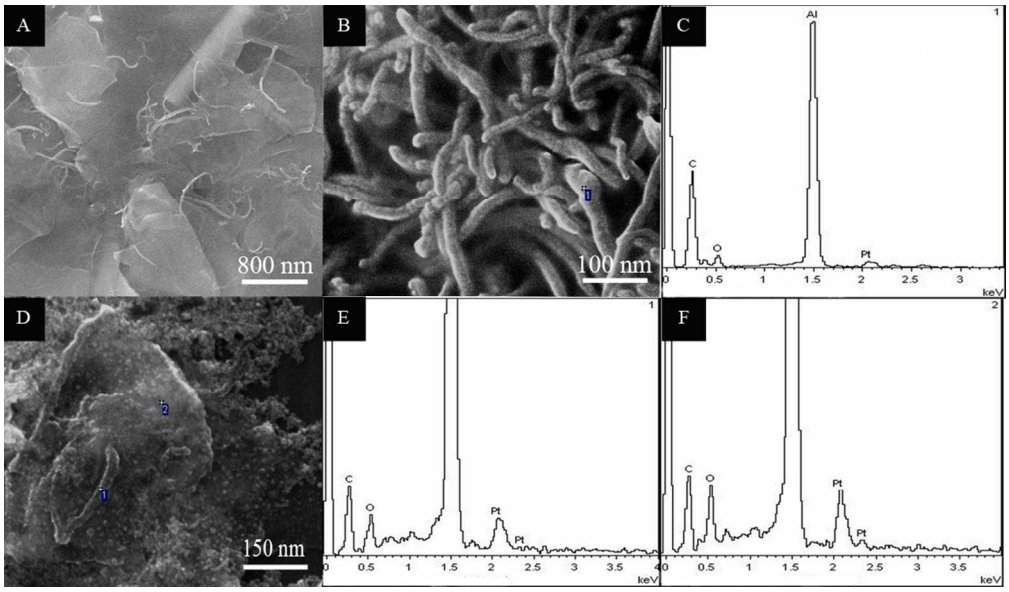

Figure 1
99x57mm (300 x 300 DPI)

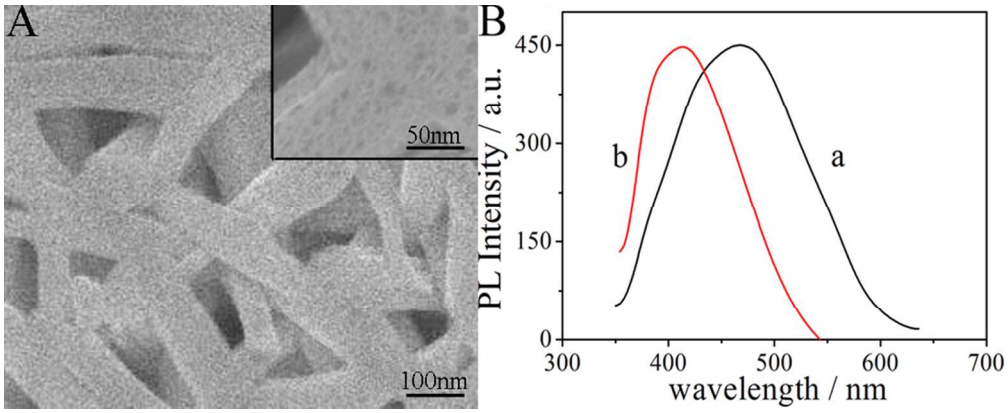

Figure 2
92x37mm (300 x 300 DPI)

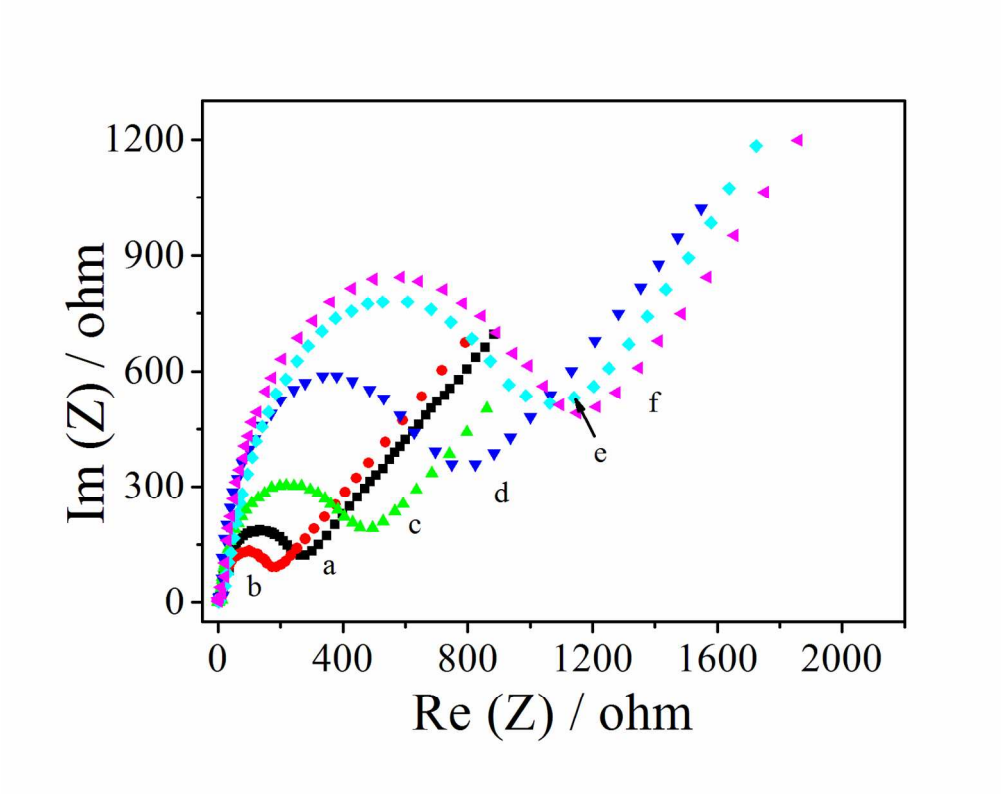

Figure 3
289x230mm (150 x 150 DPI)

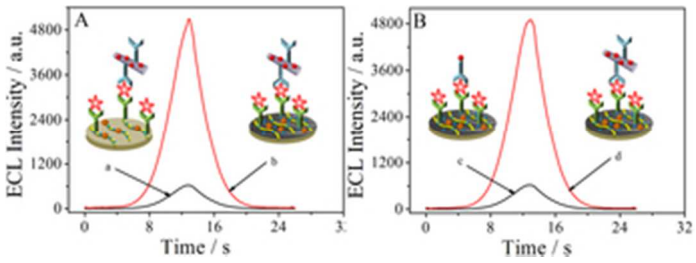

Figure 4
29x10mm (300 x 300 DPI)

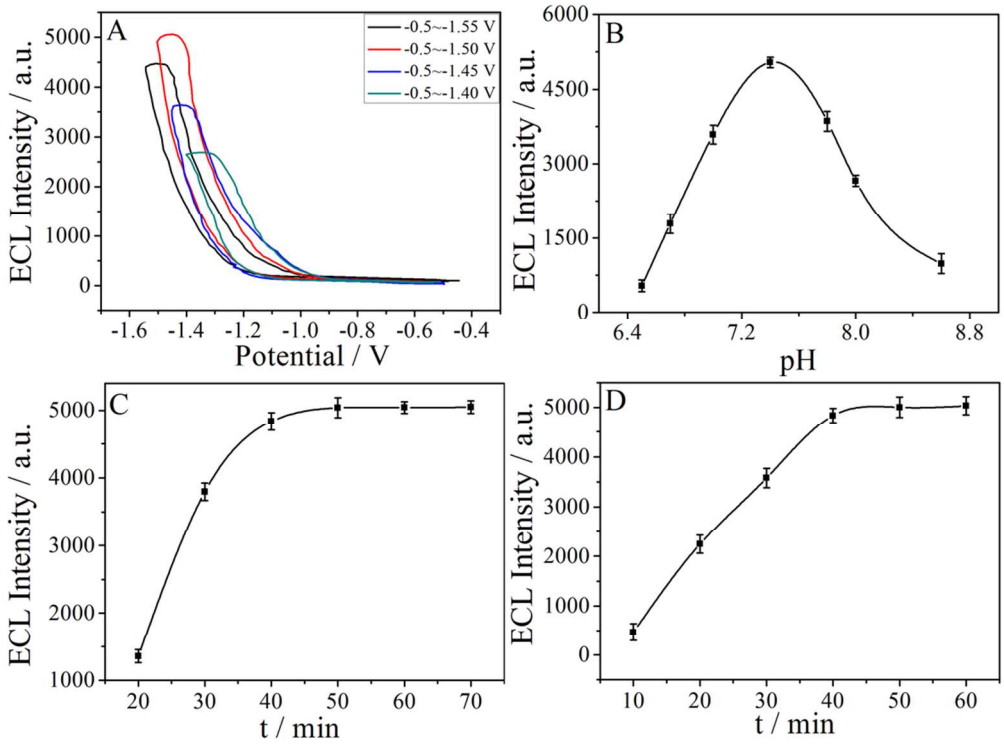

Figure 5
99x73mm (300 x 300 DPI)

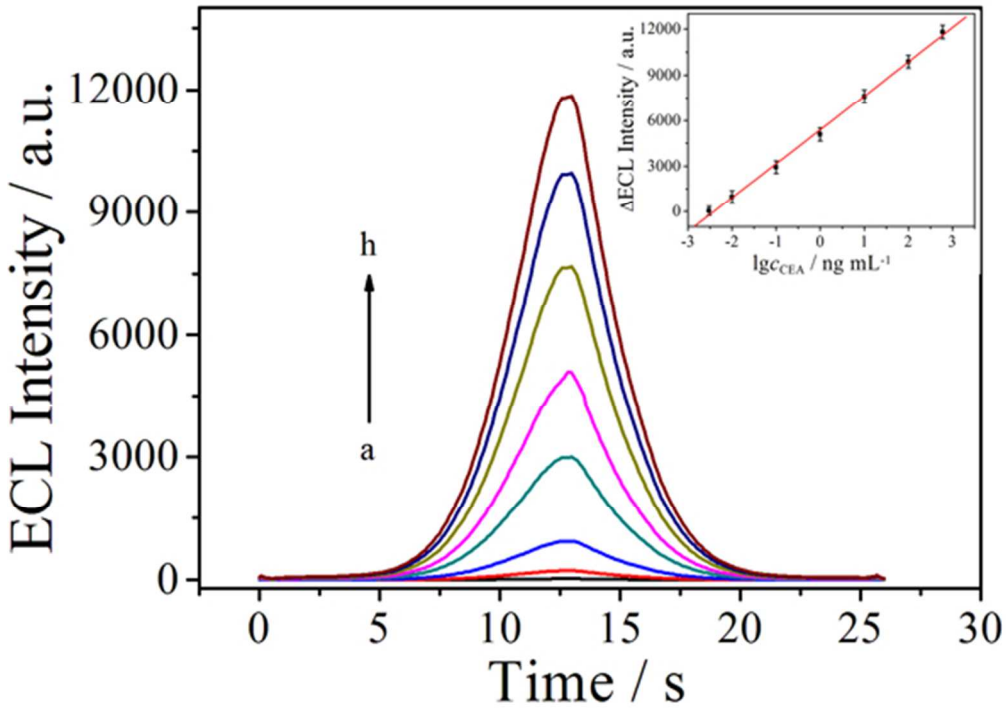

Figure 6
100x70mm (150 x 150 DPI)

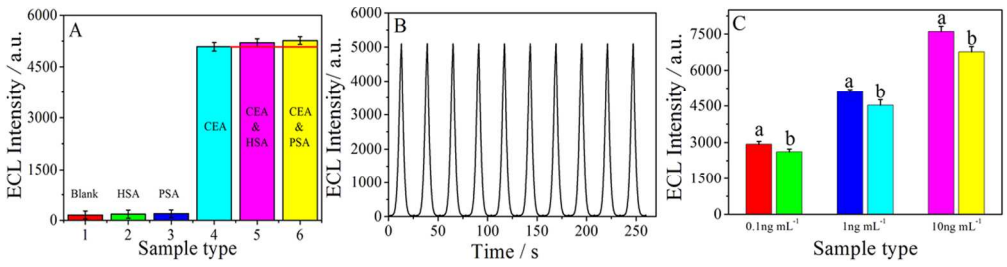

Figure 7
335x84mm (300 x 300 DPI)

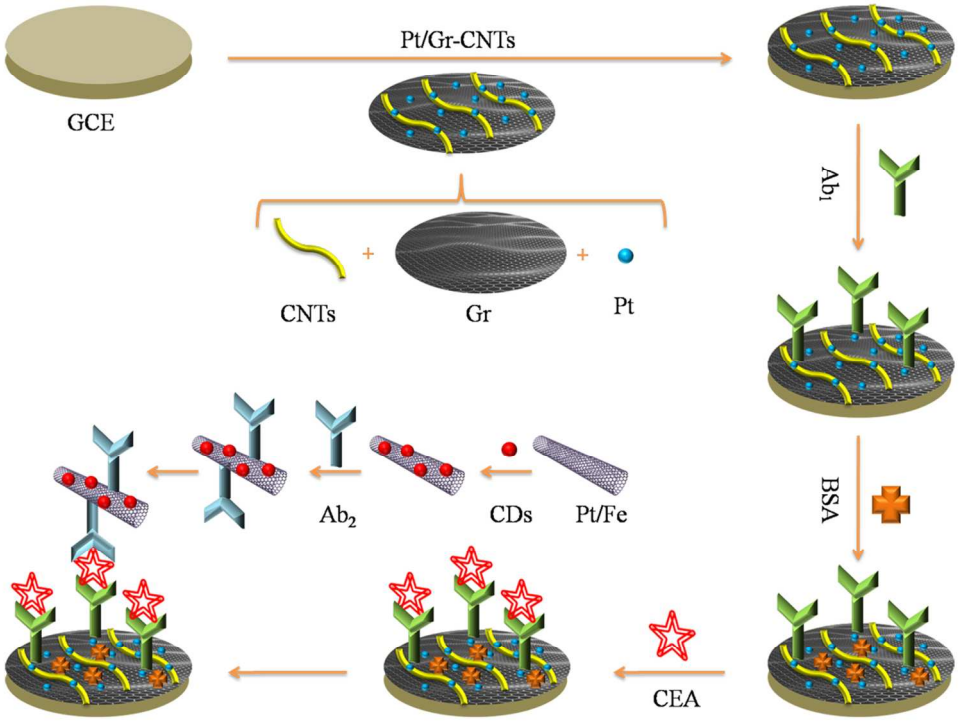

Scheme 1
111x84mm (300 x 300 DPI)

Table 1 Analytical properties of different CEA electrochemical immunosensors

Modified platform	Signal antibody	Linear range ($ng \cdot mL^{-1}$)	Detection limit ($pg \cdot mL^{-1}$)	Ref.
Graphite electrode	sol-gel	0.5-120	4	36
Screen-printed carbon electrode	nanogold	0.5-25	2.2	37
Glassy carbon electrode	nanogold	0.5-120	2	38
Carbon paste electrode	Fe_3O_4-SiO_2	1.5-60	5	39
Carbon paste electrode	Fe_3O_4-SiO_2	1.5-200	5	40
Glassy carbon electrode	Pt/Fe@CDs	0.003-600	0.8	This work

Table 2 Comparison of CEA detection between the proposed immunosensor and ELISA methods in CEA-spiked human serum samples

Immunosensor concentrations ($ng \cdot mL^{-1}$)				ELISA concentrations ($ng \cdot mL^{-1}$)			
Sample	Added	Found	Recoveries (%)	Added	Found	Recoveries (%)	Relative deviation (%)
1	0.5	0.518	103.6	0.5	0.522	104.4	-0.77
2	1.0	0.977	97.7	1.0	0.988	98.8	-1.13
3	2.0	1.976	98.8	2.0	2.028	101.4	-2.63
4	3.0	2.954	98.5	3.0	3.023	100.8	-2.34